Composite Structures 367 (2025) 119265



Contents lists available at ScienceDirect

Composite Structures

journal homepage: www.elsevier.com/locate/compstruct





The effects of environmental conditions on the failure of double lap composite joints with different overlap lengths and adherend thicknesses

Aakash Paul [a], Xiaodong Xu [b,*], Takayuki Shimizu [c], Michael R. Wisnom [a]

[a] Bristol Composites Institute, University of Bristol, University Walk, Bristol BS8 1TR, UK
[b] Centre for Aeronautics, Faculty of Engineering and Applied Sciences, Cranfield University, Cranfield MK43 0AL, UK
[c] Research & Innovation Centre, Mitsubishi Heavy Industries, LTD. 10, Oye-cho, Minato-ku, Nagoya 455-8515, Japan

ARTICLE INFO

Keywords:
Bonding
Delamination
Environmental degradation
Analytical modelling
Joints

ABSTRACT

This paper provides a comprehensive study of the effects of environmental conditions on the failure of Double Lap Joints (DLJ) with composite adherends of different overlap lengths and thicknesses. The environmental conditions tested are Room Temperature Dry (RTD), Hot Temperature Dry (HTD) and Hot Temperature Wet (HTW). The mechanical properties of both the adhesive and composite adherends were characterised at these environmental conditions, showing conflicting trends. A new way of presenting the data based on simple calculations of strength or fracture dominated failure allows all the data to be shown on a single plot, and satisfactorily explains the failure modes, failure loads and opposite trends observed for a total of 13 DLJ configurations tested at the three environmental conditions.

1. Introduction

An adhesively bonded joint offers lower weight, a more uniform stress distribution and enhanced fatigue life when compared to the traditional mechanical fastening methods [1], therefore it is an attractive option for aircraft designers. The use of carbon fibre composites as adherends for adhesive joints is also an attractive option for engineers due to the advanced properties of composites, such as high strength to weight ratio and improved fatigue life compared to metallic structures [2].

It is important to understand how adhesive joints fail. Different types of failures for adhesive/composite systems and the means of accurately characterising the failures are described in the ASTM D5573 standard [3]. The failure load of a typical joint can be influenced by several factors, such as the adherend/adhesive properties, the thickness of the adherend/adhesive, adherend stacking sequence, the overlap length of the joint and environmental conditions [4].

Numerous authors have investigated the overlap length effects for adhesive joints, and the failure load was generally found to increase but not necessarily in proportion to the overlap length. This is often accompanied by a change of failure mode. Kupski et al. [5] tested single lap joints of two overlap lengths with $[0/90]_{4s}$ and $[90/0]_{4s}$ stacking sequences, and found cohesive failure with 0° surface plies but delamination migration with 90° surface plies. In both cases, the failure load increases with overlap lengths and the failure mode remains unchanged. Machado et al. [6] used unidirectional single lap joints to investigate the overlap length effects on bonded joints. They found the failure mode changes from partial cohesive failure to delamination as the overlap length increases, and the failure load increases but not in proportion. Banea et al. [7] studied multi-material bonded single-lap joints with different overlap lengths. They observed cohesive failure in all cases, and the failure load increases with overlap lengths. Lee et al. [8] concluded for adhesively bonded composite single lap joints, with a stacking sequence of $[45/0/-45/90]_s$ that the failure mechanism changes from cohesive failure to delamination when increasing the overlap length, and failure load increases. The above studies mostly used single-lap joints, and all tested were done at room temperature. They showed that different failure modes in bonded joints often switch at different overlap lengths, but the reasons for this have not been fully explained.

The effect of environmental conditions such as elevated temperature or humidity levels is also not very clear. Strengths usually decrease, but fracture properties may be similar or sometimes even increase, giving rise to potentially conflicting results for joint performance. Machado et al. [6] used unidirectional single lap joints to investigate the hygrothermal aging effect on bonded joints and found the failure mode

* Corresponding author.
E-mail address: xiaodong.xu@cranfield.ac.uk (X. Xu).

https://doi.org/10.1016/j.compstruct.2025.119265
Received 25 October 2024; Received in revised form 2 May 2025; Accepted 7 May 2025
Available online 10 May 2025
0263-8223/© 2025 The Author(s). Published by Elsevier Ltd. This is an open access article under the CC BY license (http://creativecommons.org/licenses/by/4.0/).

changes from partial cohesive failure to delamination at shorter overlap length. The failure load also decreases in hygrothermally aged joints with a larger reduction in longer overlaps. Liu et al. [9] conducted double-lap tests of adhesively bonded unidirectional joints at different environmental conditions. They found a reduction of tension strength when the joints were exposed to moisture, a further reduction at elevated temperature and the greatest reduction under hot wet conditions. Moisture was also found to promote cohesive failures. Viana et al. [10] conducted dog-bone tests on adhesives for samples conditioned for different time periods and at different temperatures. A significant decrease in strength was found as the moisture absorption caused plasticisation and increased ductility. For conditioned specimens tested at a high temperature, a further decrease in strength was observed as the test temperature approached the Tg of the material.

Prolonged exposure to high temperatures also affects the adhesive strength and fracture properties. Hot temperature dry tests on modified epoxy adhesives were conducted by da Silva and Adams [11]. A decrease in both tensile and shear modulus and strength was reported with increased temperature. A sharp fall in strength was also reported once the test temperature exceeded the Tg (155 °C). Banea et al. [12] conducted both G_{IC} and G_{IIC} characterisation tests for epoxy adhesives with metallic adherends at different temperatures. The G_{IC} increased slightly with temperature for the adhesive due to the increased ductility enhancing the plastic deformation at the crack. However, once the Tg of the adhesive was approached, a drop in G_{IC} was reported. For Mode II, a similar conclusion was found in that the G_{IIC} increased initially with increasing temperature due to the increased ductility of the adhesive and then decreased as the testing temperature approaches the Tg of the adhesive. Chai et al. [13] also backed this up, reporting that G_{IIC} decreased between $0.7 < T/Tg < 1$. Viscoelasticity and creep effects are also more significant due to the increased mobility of the adhesive polymer chains at high temperatures [14].

The composite adherends are also affected by moisture and temperature. The mechanical properties of the composites degrade with moisture absorbed due to the plasticisation of the epoxy matrix or degradation of the fibre/matrix interface [15,16]. Carbon fibres do not absorb significant moisture. Wong [17] conducted mechanical tests for composites at different absorbed moisture contents. The author concluded that the transverse strength of the composites degraded while in the longitudinal direction only a small decrease in strength was observed. For G_{IC}, no significant difference was reported with increasing moisture content, while G_{IIC} decreased. Coronando et al. [18] concluded that for a carbon/epoxy system, increasing the testing temperature, to up 90 °C increased the ductility of the matrix. The increase in G_{IC} was more noticeable for the fatigue test than the static test at higher temperatures. The change of material properties can lead to a change of failure modes. For example, the temperature effects on adhesively bonded composite joints were studied by Khafagy et al. [19]. The tensile strength decreased with increasing temperatures, with a mixed (adherend/composite) failure reported at room temperature and cohesive failure at higher temperatures.

The failure mechanisms at different environmental conditions are so far not well understood. The existing industrial approach is to apply a knock-down factor for the design to take account of temperature and moisture effects and rely on large scale testing. The purpose of this current research is to understand the failure modes at different environmental conditions and the effects of overlap length and adherend thickness. A new approach is proposed considering the effects of both adhesive strength and toughness. It shows why joint strength in hot-wet conditions is lower than in room temperature dry conditions in some cases, but higher in others, which cannot be explained by existing approaches. It enables all the data across a total of 13 joint configurations and three environmental conditions to be put on a single plot, which is useful to guide the design of double lap joints. Such a comprehensive study has not been done for composite double-lap joints.

2. Experimental setup

The material for the composite adherends used was Hexcel's HexPly® IM7/8552 carbon/epoxy prepreg with a nominal thickness of 0.125 mm. The adhesive used was Hexcel's Redux® 319 367 g/m^2 unsupported film adhesive with a nominal cured thickness of 0.2 mm and no carrier.

2.1. Double lap joints manufacturing

The schematic for the typical Double Lap Joint (DLJ) is shown in Fig. 1. The layup of the IM7/8552 laminates was done first. The stacking sequence of the laminates was Quasi-isotropic (QI), e.g. $[0/45/90/-45]_{2s}$ for the 4 mm inner adherend case, and $[0/45/90/-45]_s$ for the 2 mm inner adherend case. After surface treatment of the QI laminates by grit blasting, they were bonded with the Redux® 319 film adhesive to form two half joints separated by release film in the configuration shown in Fig. 2. Two spacers made of the same composite and adhesive film and one spacer of adhesive only were used to ensure constant adhesive thickness was achieved throughout the joint and minimum leakage of adhesive during the curing process, and to allow flat tooling. The composite spacers were pre-cured but the adhesive spacers were co-cured. The release film ensured that after the curing process, the spacers could be separated from the adherends. After the secondary bonding process of the half joints was completed, paste adhesive (Huntsman's Araldite® 2014–1) was used to bond them and form a symmetrical DLJ. For example, an approximately 4 mm thick inner adherend at the midplane is made up of two 2 mm laminates bonded together as shown in Fig. 1.

2.2. Specimen configurations

A total of 13 joint configurations were tested, with overlap lengths from 12 mm to 36 mm under Room Temperature Dry (RTD), Hot Temperature Dry (HTD) and Hot Temperature Wet (HTW) environmental conditions for both 2 mm and 4 mm inner adherend thickness, as shown in Table 1. Due to time constraints only the 36 mm overlap length was tested for the 2 mm inner adherend at HTD.

2.3. Specimen moisture conditioning

The moisture conditioning was carried out at 80 °C at 85 % relative humidity for the joints according to the ASTM D5229 standard [20]. The environmental chambers used were the Vötsch VC 7034 and the CM Envirosystems. The specimens were weighed using a universal weighing scale with a precision of 0.0001 g. The moisture uptake readings were taken every week for the first five weeks, and then taken every fortnight. The bonded joints were conditioned for four months or until 1 % moisture weight gain was achieved. The weights of all specimens were recorded before and after conditioning, with 0.8 % weight gain in composites, 1.8 % weight gain in adhesive at saturation.

2.4. Testing configuration

For the RTD case an Instron 100 kN hydraulically driven machine was used for tensile testing. The HTD and HTW tests were conducted at 80 °C using a thermal chamber and a mechanically driven Zwick 50 kN test machine. Testing was conducted under displacement control at a loading rate of 0.5 mm/min and four specimens were tested for each configuration. The DLJ strength was based on the maximum load before catastrophic failure and the nominal specimen width. The primary failure mechanism was examined using a Photron high-speed camera. The high-speed camera video was taken at 80,000 frames per second.

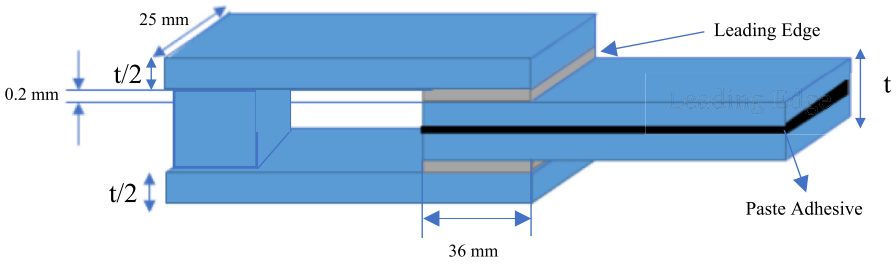


Fig. 1. Schematic and dimensions of the longest double lap joint (not to scale).

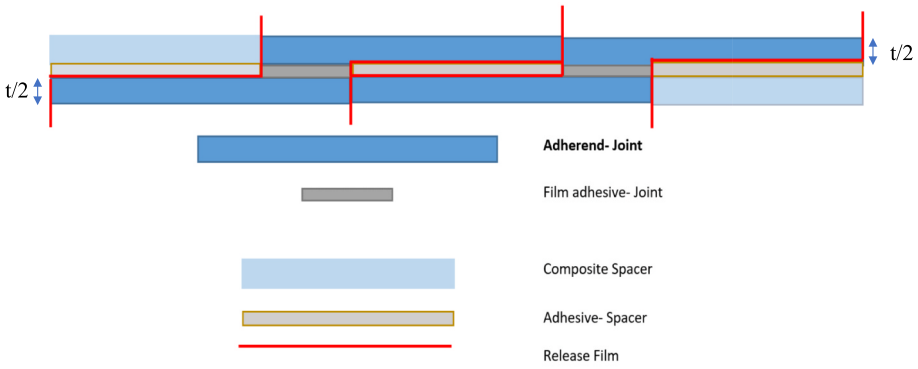


Fig. 2. Schematic of the initial bonding configuration for the two half joints before combining them to make a symmetrical double lap joint.

Table 1
Test matrix of 13 DLJ configurations and three environmental conditions.

	2 mm Inner Adherend			4 mm Inner Adherend	
Overlap Length	12 mm	24 mm	36 mm	12 mm	36 mm
RTD	✓	✓	✓	✓	✓
HTD			✓	✓	✓
HTW	✓	✓	✓	✓	✓

3. Double lap joints results

All the experimental results for the DLJ are summarised in this section. Fig. 3a and Fig. 3b present the effects of increasing overlap length on DLJ strength for the 2 mm and 4 mm inner adherend cases, respectively. The results show opposite trends for the effect of conditioning on 12 mm and 36 mm long joints. Comparing the 2 mm and 4 mm inner adherend cases shows that increasing adherend thickness increased the DLJ strength.

3.1. Room temperature dry

In Fig. 3a at RTD, there is no significant difference in strength with increased overlap length for the 2 mm inner adherend thickness. Increasing the overlap length for the 4 mm inner adherend case increased the DLJ strength, as shown in Fig. 3b. The strengths of the 4 mm inner adherend cases were higher than for 2 mm at both lengths.

3.2. Hot temperature dry

At HTD, Fig. 3a and Fig. 3b show that increasing the inner adherend thickness from 2 mm to 4 mm resulted in a significant increase in DLJ strength for the 36 mm overlap length case. Increasing the overlap length for the 4 mm inner adherend case significantly increased the DLJ

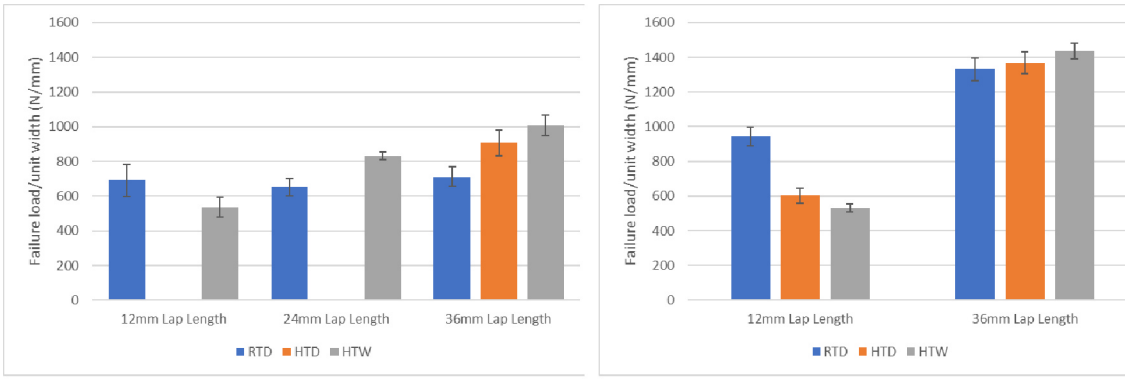


Fig. 3. DLJ test results summary.

strength, in contrast to the results at RTD.

3.3. Hot temperature wet

Increasing the overlap length for both the 2 mm and 4 mm inner adherend case at HTW increased the DLJ strength as shown in Fig. 3a and Fig. 3b. The strength for the 4 mm inner adherend case was higher than for 2 mm inner adherend and 36 mm overlap, but similar for 12 mm overlap.

4. Results analysis

4.1. Analysis based on simple failure criteria

During the DLJ tests at different environmental conditions, two different trends were observed. The shortest overlap length cases (12 mm) decreased in strength with increased temperature and moisture whereas the joint strength increased for the longer overlap length cases (24 mm and 36 mm). Simple analytical failure criteria can be applied to the DLJ test results to help explain the trends in DLJ strength at different environmental and geometrical conditions. They are used to describe the two different factors controlling the DLJ strength: the shear strength for bondline yielding and the critical strain energy release rate for propagation of debonding as shown in Fig. 4. The shear strength of the adhesive provides an upper bound on the joint strength, with the maximum load increasingly linearly with overlap length, represented by the blue line in Fig. 4. As the length and load that can be transferred increases, a limit is reached where the energy release rate exceeds the value required to propagate debonding along the joint. No further load can be carried, and the joint strength reaches a plateau, as represented by the red line in Fig. 4. In this simplified picture failure of short overlap joints is controlled by the shear strength assuming a total yielding of the adhesive, whereas failure of joints with long overlaps is controlled by a crack in the adhesive fillets propagating according to fracture mechanics. In reality, most cases are influenced by both mechanisms. Shear lag analysis by Volkersen [21] also predicts a plateau on the DLJ strength with increasing overlap length, but at a very low failure load as it assumes a linear elastic response. Also, since it is based on the adhesive strength, it cannot explain the increase in joint strength under HTW conditions for the longer overlap cases.

To apply this simple analysis quantitatively, the shear strength of the adhesive, S, was used to estimate the expected failure load per unit width, P_w, as shown in Equation (1), where L is the overlap length. The material properties are summarised in Table 2. Some of these values were estimated rather than measured, and so the calculated joint strengths are subject to some uncertainty, but are considered adequate to illustrate the principle and explain the trends.

$$P_w = 2SL \tag{1}$$

To obtain the expected failure load for debonding, a simple fracture mechanics approach based on the strain energy release rate (G) was used in Equation (2). It was previously used for centre cut-ply laminates [22] and is analogous to an equation originally derived for cracked lap-shear specimens [23]. Equation (2) represents the strain energy release rate as debonds propagate symmetrically along the joint, increasing the stress in the single adherend and simultaneously decreasing the stress in an equal length of the double adherends. The joint is assumed to be long, with the local stress field at the tip of the crack remaining the same, and just translating with the crack propagation.

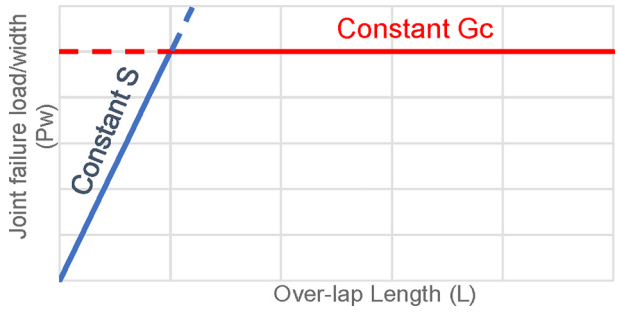


Fig. 4. Schematic of shear strength (blue) versus fracture (red) controlled joint failure.

Table 2
Material properties under different environmental conditions.

	RTD	HTD	HTW
Quoted shear strength (MPa) [26]	51.2	35[a] (est.)	28[b] (est.)
G_{IC} of adhesive (N/mm)	0.89 [24]	1.05 [26]	1.13 [26]

[a] In the absence of the HTD shear strength data at 80°C, a rough estimate was taken, using linear interpolation from the datasheet values at 22°C and 150°C.
[b] The HTW shear strength value was from the estimated HTD shear strength at 120°C. This approach was taken as the glass transition temperature (Tg) of a material decreases with moisture. Hence, it was postulated that the difference between the test temperature (80°C) and Tg at wet conditions would be similar to the HTD shear strength at 120°C.

$$G = \frac{\sigma_0^2 t}{8E} \tag{2}$$

The Young's modulus in the loading direction is $E = 61.6$ GPa which is assumed to be constant at different environmental conditions. The applied stress on the inner adherend is σ_0. The term t is the thickness of the inner adherend and the total thickness of the joint is $2t$, as the inner adherend is twice as thick as the outer as shown in Fig. 1.

The assumption of this method is that the overlap is long, and effects of the local stress field around the crack tip do not affect the strain energy release rate when the debonding propagates, as the stress field moves along the specimen, unloading the inner adherend of thickness t and loading an equivalent length of the two outer adherends each of thickness $t/2$ [22].

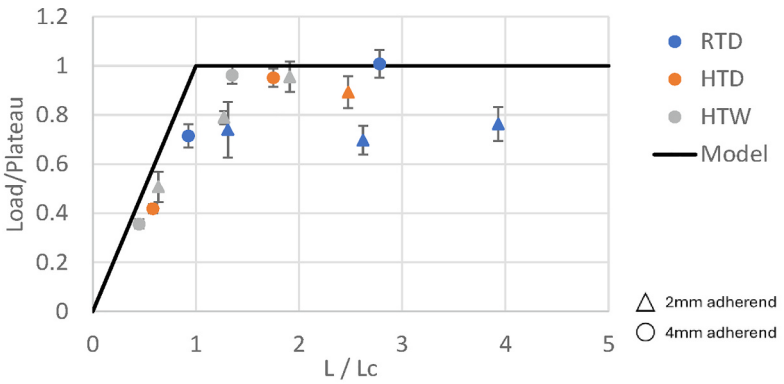
Rearranging Equation (2), the fracture energy, G_C, was then used to calculate the failure load per unit width according to Equation (3), using the material properties in Table 2.

$$P_w = 2\sqrt{2G_C Et} \tag{3}$$

The results are plotted in Fig. 5a and b, compared against two lines: a line of increasing strength with overlap length based on the strength criterion, Equation (1), and a constant strength based on the fracture criterion, Equation (3). The point of intersection of the two lines is representing the critical overlap length L_c, which is determined by equating Equations (1) and (3) and rearranging to get Equation (4).

$$L_c = \frac{\sqrt{2G_C Et}}{S} \tag{4}$$

Results are normalised based on the overlap length divided by the critical overlap length, L_c and the failure load per unit width divided by the value of P_w from Equation (3) to allow the different adherend thicknesses and environmental conditions to be presented on the same plot. The failures that fall between 0 and L/L_c are expected to be controlled by the shear strength of the adhesive whereas failures occurring above L/L_c are expected to be controlled by the fracture energy, G_C. The fracture energy value used here is Mode I fracture energy of the adhesive, G_{IC}. This is because the fracture initiates from the adhesive fillet, which is primarily under Mode I loading. The fracture then propagates in the bondline initially before migrating into the composites. The adhesive G_{IC} of 0.89 N/mm at RTD was from Ref. [24], and those at HTD and HTW were measured in double cantilever bean and end notched flexure tests of bonded unidirectional specimens as shown



a) Results comparison

	t	Overlap	l/lc	P/Ppl	S.D	No. of Specimens
RTD	2	12	1.31	0.74	0.11	4
	2	24	2.62	0.70	0.06	4
	2	36	3.93	0.76	0.07	3
	4	12	0.93	0.72	0.05	4
	4	36	2.78	1.01	0.06	4
HTD	2	36	2.48	0.89	0.06	3
	4	12	0.58	0.42	0.02	4
	4	36	1.75	0.95	0.04	3
HTW	2	12	0.64	0.51	0.06	5
	2	24	1.27	0.79	0.03	4
	2	36	1.91	0.96	0.06	4
	4	12	0.45	0.36	0.02	5
	4	36	1.35	0.96	0.04	4

b) Results summary

Fig. 5. Normalised plots of DLJ failure against simple analytical criteria.

in Table 2.

The first three points on the left between 0 and $L/L_c = 1$ are the cases with 12 mm overlap length at HTD and HTW, where the failure is limited by the shear strength of the adhesive. The other cases where failures occur above $L/L_c = 1$ are fracture energy dominated, and so do not reach the potential loads based on the strength of the adhesive. A baseline case for each of the two types of failure mode is studied in the next two sections to understand this behaviour in more detail.

4.2. *Fracture-controlled failure mode*

The 4 mm adherend, 36 mm overlap length case at RTD was chosen as the 1st baseline case to examine a fracture-controlled failure mode. A linear force–displacement curve was observed before sudden and catastrophic failure. The fracture surface and corresponding failure schematic are shown in Fig. 6, where the dotted line in the schematic represents the primary crack propagation path during failure. The fracture surface image shows the two bonded inner adherend/outer adherend interfaces with fibres visible on all interfaces, indicating migration into the surface 0° plies. The images shown are post failure of

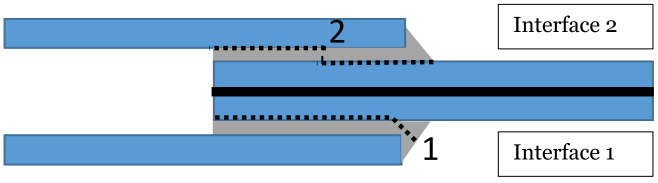


Fig. 7. Failure process schematic of the 1st baseline case.

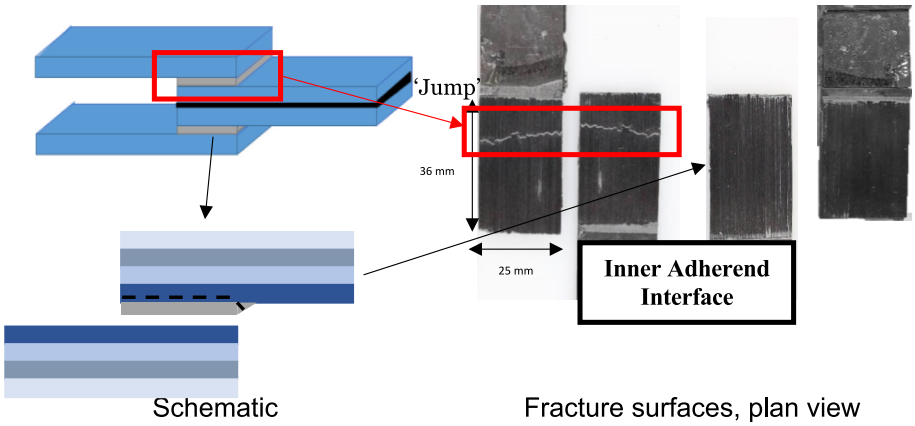


Fig. 6. Failure schematic and fracture surfaces for failure within composite in a fracture-controlled case (4 mm inner adherend, 36 mm RTD case).

the whole bondline, hence include secondary mechanisms such as the 'jump' as shown in Fig. 7.

The primary failure mechanism is explained based on high-speed camera images in Fig. 8. The images do not show any indication of crack initiation during the initial stages of loading. Analysing the frame before catastrophic failure in Fig. 8, an angle-crack is visible within the adhesive fillet and a small crack near the interface with the surface 0° ply of the composite inner adherend. It was not clear whether the crack initiated within the adhesive fillet or at the composite interface first, as cracks appeared in both materials simultaneously. As the failure was sudden and catastrophic and the high-speed camera did not pick up the failure sequence, it was postulated that the crack initiated at the adhesive fillet due to the high peel component at the leading edges of the DLJ. It then propagated into the bondline before migrating into the surface 0° ply of the inner adherend. A large process zone is expected due to the high toughness and relatively low strength of the adhesive. This means that deformation in the adhesive and bondline before and immediately after cracking in the fillet affects the load transfer between the adherends and hence the energy available to drive debonding, justifying the use of Equations (2) and (3).

Fig. 6 describes the failure mechanisms and shows a 'jump' pattern on the fracture surface. Why this occurred is explained through analysing the failure from the high-speed camera. The DLJ has two inner-adherend/outer adherend interfaces as labelled in Fig. 7, with an overview of the mechanisms that happen in sequence from No. 1 and No. 2. The primary failure mechanism is represented by Mechanism No. 1 in the schematic in Fig. 7. This is fracture controlled because a crack is formed in the adhesive fillet and migrates into the composite. During the primary failure mechanism, due to asymmetry formed by the initial crack propagation, delamination started to initiate from the leading edge and propagated within the surface 0° plies. Then cracks were present at the outer adherend at the rear end of the second interface and at the forward adhesive/inner adherend interface. When the delamination path from the inner adherend leading edge and outer adherend trailing edge at the second interface approached each other, the cracks joined up by fracture of the adhesive (Mechanism No. 2). This is represented by the 'jump' pattern on the fracture surface as highlighted on the schematic of strength versus fracture controlled joint failure in Fig. 6.

4.3. Strength-controlled failure mode

Next, an example of the failure controlled by the strength of the adhesive is discussed, referred to as strength controlled. For this case, the 4 mm inner adherend, 12 mm overlap length at HTD was used as the 2nd baseline case to explain the failure mechanism. The failure was sudden and catastrophic. The typical fracture surface and corresponding failure schematic for this case are shown in Fig. 9. The fracture surface shows the post failure surface of the whole bondline and does not indicate the sequence of the failure. The failure schematic shows the primary failure mechanism within the adhesive. For this case, patches of adhesive and 0° fibres were visible on both the primary fracture surfaces, different to the fracture-controlled failure mode fracture surfaces, where only the 0° fibres were visible clearly. This suggests that the adhesive in the bondline primarily influenced the failure, and this case has exhibited partial cohesive failure.

Now the failure modes for all tested environmental conditions are analysed as follows.

4.4. Room temperature dry – Failure mode

The 2 mm inner adherend results are compared against the simple criteria as plotted in Fig. 5. Analysing the results shows that at RTD, all overlap lengths fall within the area of expected failure based on fracture energy, hence explains why the strengths were similar. This is consistent with the post failure fracture surfaces as follows.

For all 2 mm inner adherend cases, the fracture surfaces show the 0° ply visible across all four fracture surfaces. This is because the crack

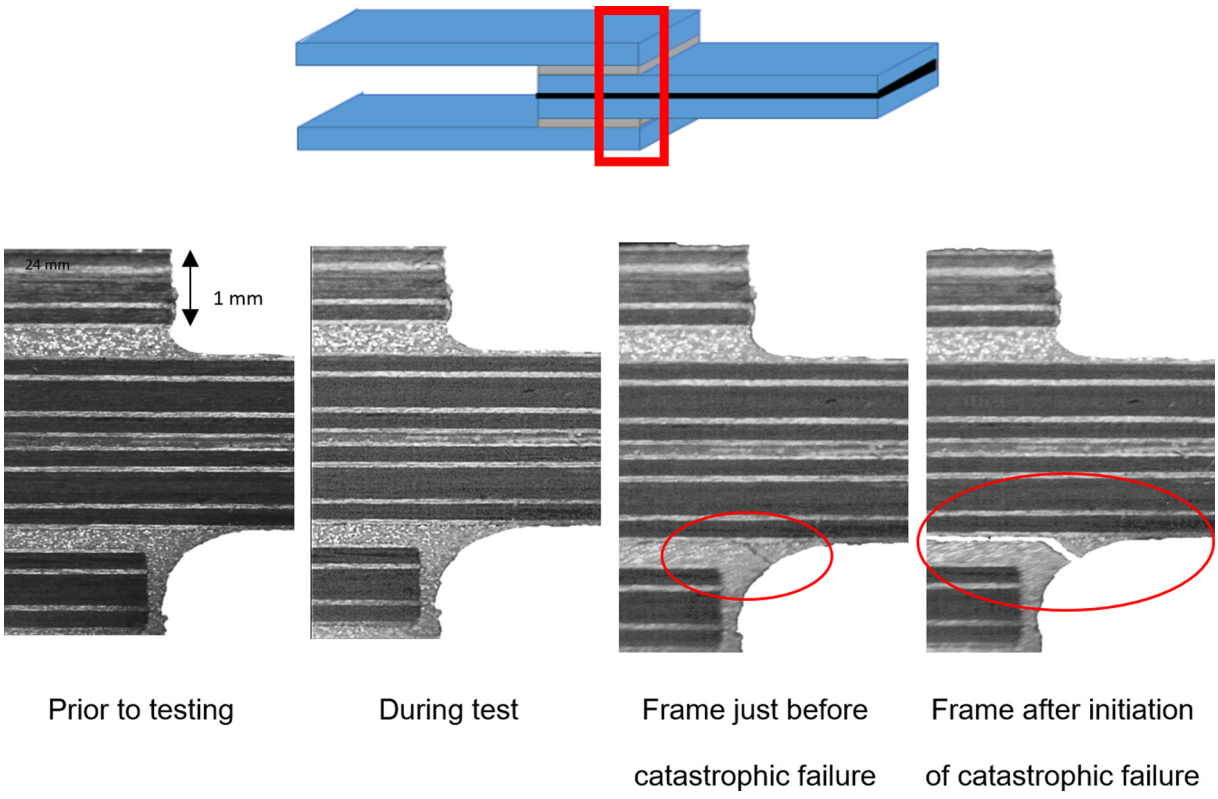


Fig. 8. High-speed camera images of fracture-controlled failure, side view.

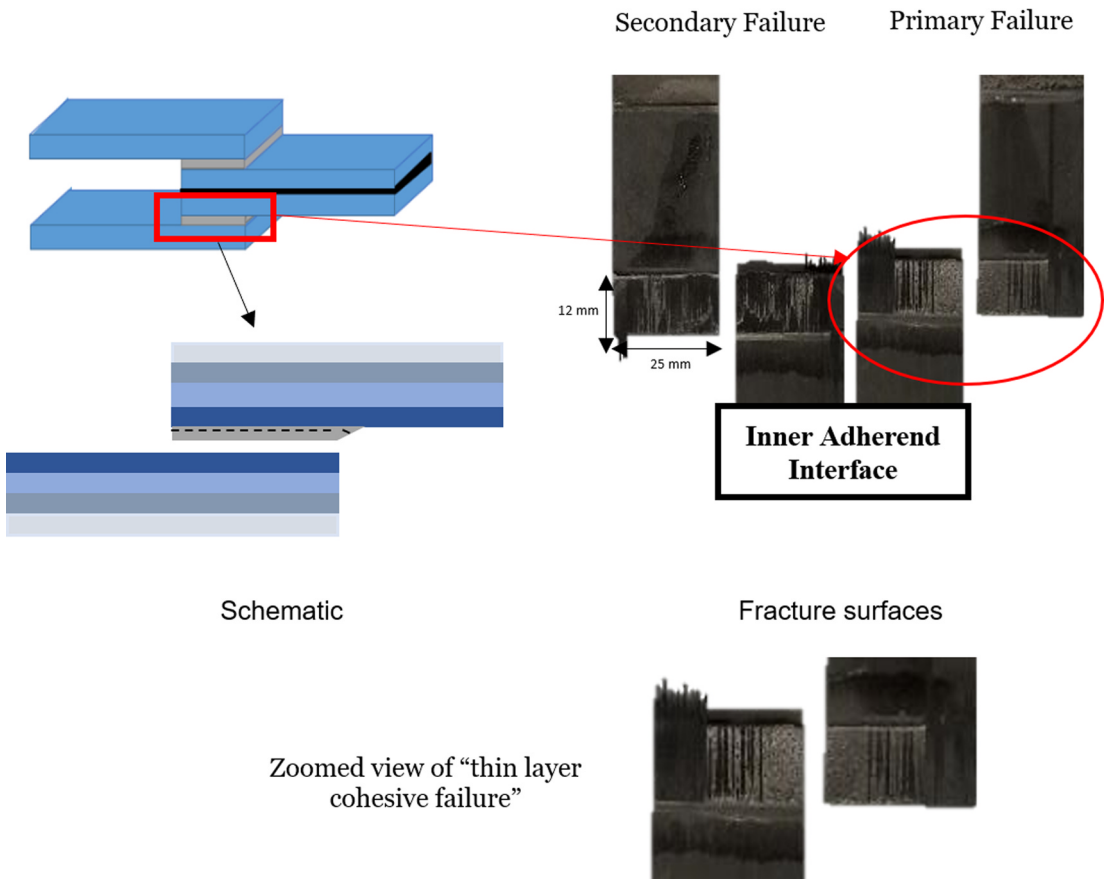


Fig. 9. Failure schematic of the 2nd baseline case and fracture surfaces for failure within adhesive and composite in a strength-controlled case (HTD, 4 mm inner adherend, 12 mm overlap length).

migrates into the composite despite the surface 0° ply orientation. Fibres broken during grit blasting surface treatments facilitate crack migration, as explained elsewhere [25]. Analysing the 2 mm inner adherend results shows that there was no significant difference in strength for the three overlap lengths tested. For all 2 mm inner adherend RTD cases, the crack initiated at the adhesive fillets and then migrated into the composite surface 0° ply.

The fracture surface images (Fig. 10) show that the 12 mm overlap length case had fragments of adhesive in grey on the fracture surface and the failure mode was not conclusive based on this observation. The 36 mm overlap length fracture surfaces show the surface 0° plies in black across all adherend/outer adherend interfaces, similar to the 2 mm inner adherend case.

The 12 mm overlap length, 4 mm inner adherend thickness case is close to the transition point between the shear-controlled and fracture-controlled failure modes, consistent with the traces of adhesive in the fracture surface for this case.

4.5. *Hot temperature dry – Failure mode*

The fracture surfaces for these cases are shown in Fig. 11. The 4 mm inner adherend with 12 mm overlap length had patches of adhesive on the fracture surface, indicating a partial cohesive failure i.e. strength-controlled failure mode. Whereas for the 36 mm overlap length, only the composite surface 0° plies were visible on the fracture surface, indicating a fracture-controlled failure mode.

Comparing the HTD results in the simple analytical plot in Fig. 5 shows the shorter overlap length case was placed in the shear failure area, below the critical overlap length. This matches the post failure fracture surface in which adhesive was observed. The analytical plot

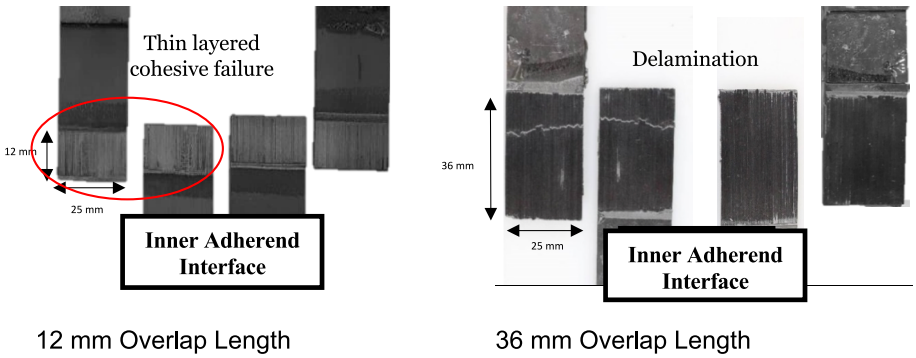


Fig. 10. Fracture surfaces for 4 mm inner adherend cases at RTD.

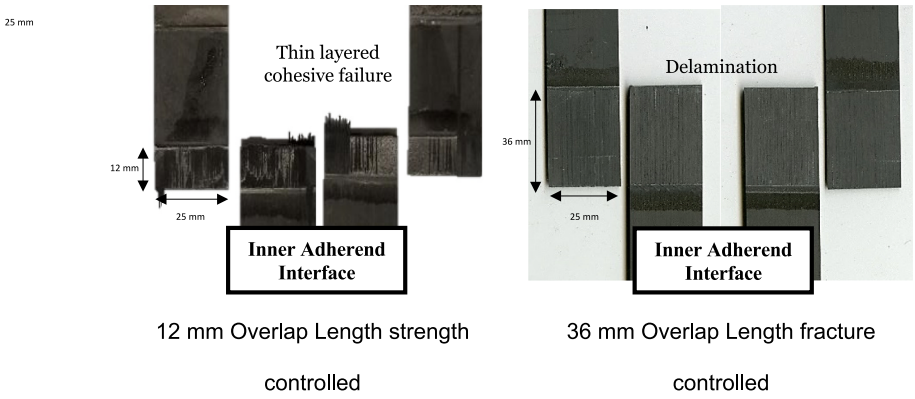


Fig. 11. Fracture surfaces for 4 mm inner adherend cases at HTD.

suggests that the longer overlap length cases for both adherend thicknesses are fracture-controlled, consistent with the fracture surfaces.

4.6. *Hot temperature wet – Failure mode*

Fig. 12 and Fig. 13 show the fracture surfaces for these cases. The 12 mm overlap length case had patches of adhesive visible on the fracture surface, indicating a strength-controlled failure mode. For the 24 mm and 36 mm overlap length cases, only the surface 0° plies were visible on the fracture surfaces, indicating a fracture-controlled failure mode.

The HTW results in the normalised simple analytical plot (Fig. 5) show the shorter overlap length cases for 2 mm and 4 mm inner adherend thicknesses placed below the critical overlap length, suggesting a strength-controlled failure, consistent with the fracture surfaces. The 24 mm and 36 mm overlap length cases were all beyond the critical overlap length, in the plateau region, suggesting a fracture-controlled failure, which matched the fracture surfaces.

5. Conclusions

The strength of double lap joints with short overlap length was found to decrease at high temperature, with a further small decrease when fully moisture conditioned. The strength of joints with longer overlap length showed the opposite trend, increasing at high temperature, with a further increase when wet, especially with thinner adherends. The reason for this is because the strength of the short overlap joints is dominated by the shear strength of the adhesive, which reduces under hot and wet conditions. On the other hand the strength of the longer overlap joints is fracture controlled, dominated by the Mode I fracture toughness of the adhesive, which increases under hot and wet conditions. This also explains why the overlap length of the thinner adherend joints at room temperature does not significantly affect the strength, as they are all long enough to be fracture controlled. But under hot and wet conditions the double lap joint strength does increase with overlap length as the shorter joints are strength controlled. The appearance of the fracture surfaces for these cases confirms the above explanation. A new way of presenting the results was introduced based on the normalised load and overlap length, which allowed all the data to be shown

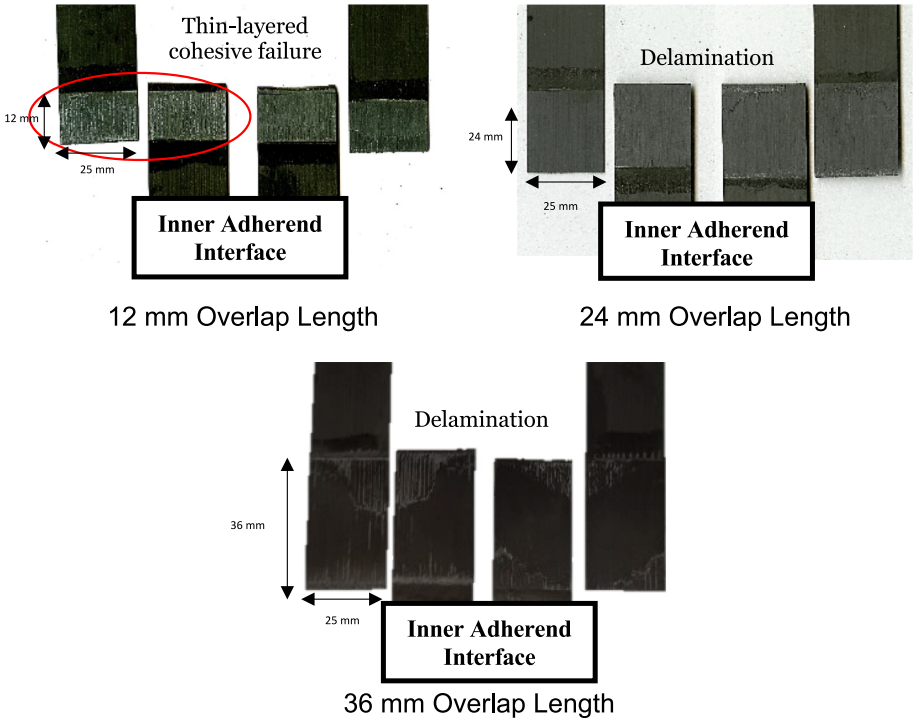


Fig. 12. Fracture surfaces for 2 mm inner adherend cases at HTW.

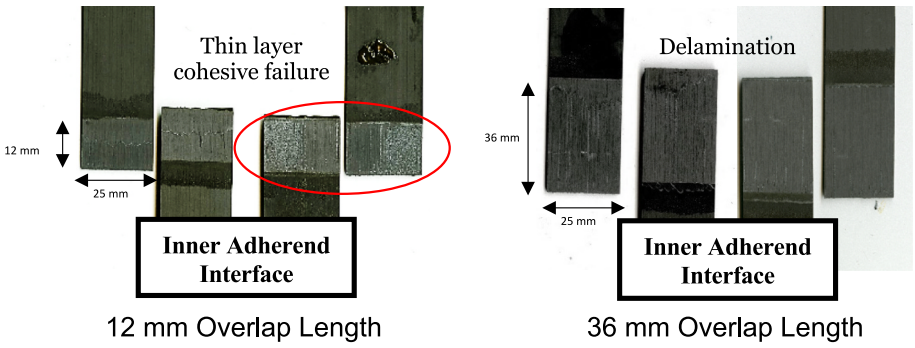


Fig. 13. Fracture surfaces for 4 mm inner adherend cases at HTW.

on a single plot. It is proven to be a useful tool to help explain these conflicting trends across a wide range of joint configurations at three different environmental conditions.

CRediT authorship contribution statement

Aakash Paul: Writing – original draft, Visualization, Validation, Investigation, Formal analysis, Data curation. **Xiaodong Xu:** Writing – review & editing, Supervision, Methodology, Investigation, Conceptualization. **Takayuki Shimizu:** Project administration, Funding acquisition, Conceptualization. **Michael R. Wisnom:** Writing – review & editing, Supervision, Funding acquisition, Conceptualization.

Declaration of competing interest

The authors declare that they have no known competing financial interests or personal relationships that could have appeared to influence the work reported in this paper.

Data availability

The data that has been used is confidential.

References

[1] Harris JA, Adams RD. An assessment of the impact performance of bonded joints for use in high energy absorbing structures. Proc Inst Mech Eng C J Mech Eng Sci 1985;199:121–31. https://doi.org/10.1243/PIME_PROC_1985_199_102_02.
[2] Adams RD, Comyn J, Wake WC. Structural adhesive joints in engineering. London: Chapman & Hall; 1997.
[3] ASTM D5573 - 99. Standard Practice for Classifying Failure Modes in Fiber-Reinforced-Plastic (FRP) Joints. 2019.
[4] Wei Y, Jin X, Luo Q, Li Q, Sun G. Adhesively bonded joints – A review on design, manufacturing, experiments, modeling and challenges. Compos B Eng 2024: 111225. https://doi.org/10.1016/j.compositesb.2024.111225.
[5] Kupski J, Teixeira de Freitas S, Zarouchas D, Benedictus R. On the influence of overlap topology on the tensile strength of composite bonded joints: Single overlap versus overlap stacking. Int J Adhes Adhes 2020;103:102696. https://doi.org/10.1016/j.ijadhadh.2020.102696.
[6] Machado JJM, Marques EAS, Barbosa AQ, da Silva LFM. Effect of hygrothermal aging on the quasi-static behaviour of CFRP joints varying the overlap length. Compos Struct 2019;214:451–62. https://doi.org/10.1016/j.compstruct.2019.02.035.
[7] Banea MD, Rosioara M, Carbas RJC, da Silva LFM. Multi-material adhesive joints for automotive industry. Compos B Eng 2018;151:71–7. https://doi.org/10.1016/j.compositesb.2018.06.009.
[8] Lee HK, Pyo SH, Kim BR. On joint strengths, peel stresses and failure modes in adhesively bonded double-strap and supported single-lap GFRP joints. Compos Struct 2009;87:44–54. https://doi.org/10.1016/j.compstruct.2007.12.005.
[9] Liu S, Cheng X, Zhang Q, Zhang J, Bao J, Guo X. An investigation of hygrothermal effects on adhesive materials and double lap shear joints of CFRP composite laminates. Compos B Eng 2016;91:431–40. https://doi.org/10.1016/j.compositesb.2016.01.051.
[10] Viana G, Costa M, Banea MD, da Silva LFM. Behaviour of environmentally degraded epoxy adhesives as a function of temperature. J Adhes 2017;93:95–112. https://doi.org/10.1080/00218464.2016.1179118.
[11] da Silva LFM, Adams RD. Measurement of the mechanical properties of structural adhesives in tension and shear over a wide range of temperatures. J Adhes Sci Technol 2005;19:109–41. https://doi.org/10.1163/1568561053148449.
[12] Banea MD, da Silva LFM, Campilho RDSG. Mode I fracture toughness of adhesively bonded joints as a function of temperature: Experimental and numerical study. Int J Adhes Adhes 2011;31:273–9. https://doi.org/10.1016/j.ijadhadh.2010.09.005.
[13] Chai H. The effects of bond thickness, rate and temperature on the deformation and fracture of structural adhesives under shear loading. Int J Fract 2004;130:497–515. https://doi.org/10.1023/B:FRAC.0000049504.51847.2a.
[14] Viana G, Costa M, Banea MD, da Silva LFM. A review on the temperature and moisture degradation of adhesive joints. Proceedings of the Institution of Mechanical Engineers, Part L: Journal of Materials: Design and Applications 2016; 231:488–501. https://doi.org/10.1177/1464420716671503.
[15] Shen C-H, Springer GS. Moisture absorption and desorption of composite materials. J Compos Mater 1976;10:2–20. https://doi.org/10.1177/002199837601000101.
[16] De'Nève B, Shanahan MER. Water absorption by an epoxy resin and its effect on the mechanical properties and infra-red spectra. Polymer (Guildf) 1993;34: 5099–105. https://doi.org/10.1016/0032-3861(93)90254-8.
[17] Wong KJ. Moisture absorption characteristics and effects on mechanical behaviour of carbon/epoxy composite application to bonded patch repairs of composite structures, 2013.
[18] Coronado P, Argüelles A, Viña J, Mollón V, Viña I. Influence of temperature on a carbon–fibre epoxy composite subjected to static and fatigue loading under mode-I delamination. Int J Solids Struct 2012;49:2934–40. https://doi.org/10.1016/j.ijsolstr.2012.05.018.
[19] Khafagy KH, Stoumbos TG, Inoyama D, Datta S, Chattopadhyay A. In-situ investigation of temperature-dependent adhesive properties and failure modes in composite bonded joints. Compos Struct 2022;300:116113. https://doi.org/10.1016/j.compstruct.2022.116113.
[20] ASTM D5229/D5229M A. Standard Test Method for Moisture Absorption Properties and Equilibrium Conditioning of Polymer Matrix Composite Materials. 2014.
[21] Volkersen O. Die Nietkraftvertei Iung in Zugbeanspruchten Nietverbindun- gen mit Konstanten Laschen-querschnitten. Luftfahrtforschung 1938;15:4–47.
[22] Wisnom MR. On the increase in fracture energy with thickness in delamination of unidirectional glass fibre-epoxy with cut central plies. J Reinf Plast Compos 1992; 11:897–909. https://doi.org/10.1177/073168449201100802.
[23] Johnson WS. Stress analysis of the cracked lap shear specimen: an ASTM round robin. J Test Eval 1987;15:303–24.
[24] Jeenjitkaew C. Kissing bonds in adhesive joints: a holistic approach for surface chemistry and joint mechanics. PhD. Queen Mary: University of London; 2011.
[25] Paul A, Xu X, Shimizu T, Wisnom MR. The role of broken fibres on crack migration into 0° surface plies in adhesively bonded carbon fibre composite joints. Compos Struct 2021;276:114530. https://doi.org/10.1016/j.compstruct.2021.114530.
[26] Paul A. Understanding the effects of environmental conditions on the failure of bonded joints. PhD: University of Bristol; 2020.



https://dspace.org/

The effects of environmental conditions on the failure of double lap composite joints with different overlap lengths and adherend thicknesses

Paul, Aakash; Xu, Xiaodong; Shimizu, Takayuki; Wisnom, Michael R.

2025-09-01
Elsevier
https://doi.org/10.1016/j.compstruct.2025.119265
Paul A, Xu X, Shimizu T, Wisnom MR. (2025) The effects of environmental conditions on the failure of double lap composite joints with different overlap lengths and adherend thicknesses. Composite Structures, Volume 367, September 2025, Article number 119265

Downloaded from a DSpace repository. https://dspace.org/